Electronic Structures and Li Migration in Cubic Nickel Nitrides Intercalation compounds : From First Principles Studies

H. B. Wang[1,2], X. L. Song[1,2,], Y. Xu[1,2], Z. H. Yang[3,4,*]*

[1] School of Mineral Processing and Bioengineering, Central South University, Changsha 410083, Hunan, China
[2] Key Laboratory for Mineral Materials and Application of Hunan Province, Central South University, Changsha 410083, Hunan, China
[3] Key Laboratory of Materials Design and Preparation Technology of Hunan Province ,School of Materials Science and Engineering, Xiangtan University, Xiangtan 411105, Hunan, China
[4] Key Laboratory of Low Dimensional Materials & Application Technology (Ministry of Education), School of Materials Science and Engineering, Xiangtan University, Xiangtan 411105, Hunan, China
[*]E-mail: xlsong8822@126.com, yangzhenhua@xtu.edu.cn

The electronic structure and diffusion behavior of Li intercalation in cubic Ni_4N_4 are investigated from first principles calculations. Results indicate that the optimal Li interstitial site is an octahedral interstitial site in cubic Ni_4N_4. The Li intercalation energies indicate that the maximum amount of lithium intercalation is seven and the corresponding theoretical specific capacity reaches 644.8 mAh/g, which is far higher than that of commercial graphite (theoretical specific capacity: 372 mAh/g). Moreover, the analyses of the energy bands, density of states, charge density population, and electron localization function all indicate that the bonding states are formed by the strong hybridization of the Ni 3d and N 2p orbitals. Finally, interstitial Li migration is considered. The results show that interstitial Li migration from octahedral interstitial site (O_h) site to O_h site can be fast with an energy barrier of 0.43 eV.

1. INTRODUCTION

Over the past twenty years, lithium-ion batteries (LIBs) have achieved great success due to their superior comprehensive battery performance. However, the growing demand for higher energy density and power becomes the bottleneck of the development of LIBs. [1] Thus, the electrode materials used in these LIBs have become very important. Recently, great progress has been made in

the application of new electrode materials with attractive specific capacity and excellent cycling stability as substitutes for the commercial graphite in LIBs. [2-3] Quite recently, metal nitrides, because of their high specific capacities, high electrical conductivity, and high chemical and thermal stability, are also used as high-performance electrode materials in LIBs except for carbon [4-5] and metal oxides [6-7]. Transition metal nitrides are also of great interest, in particular, for their ability to store lithium by conversion mechanism. [8-9] A majority of the developed transition metal nitrides such as TiN, [10] VN, [11] Mo_2N, [12] FeN, [13] NbN, and [14] Ta_3N [15] have often been used as anode materials in LIBs. For example, comparing the lithium storage performance of CoO, Co_3O_4 and CoN, CoN has been reported to be the best anode material among these cobalt compounds. [16] Again, Kundu's group reported that carbon-coated nano-VN delivers a sustainable capacity of ~400 mAh/g and impressive rate performance. [17] Recently, Zhang and his co-workers showed the highest first discharge capacity of 410 mAh/g for a VN-graphene composite. [18]

Recently, our group has investigated the mechanism of lithium intercalation in cubic CoN. [19] We found that ternary phase $Li_4Co_4N_4$ has the most stability with the theoretical capacity of 367 mA/g, and the Li-ion migration barrier along the path of $O_h{\rightarrow}T_h{\rightarrow}O_h$ is 0.44 eV. Motivated by the cubic CoN, here a cubic NiN as an anode material in LIBs is tried to theoretically investigate. As far as we know, some efforts have been devoted to the studies of metal nitrides. For example, Li-ion diffusion is calculated to be $0.638{\times}10^{-14}$ m^2s^{-1} for LiNiN. [20] Also, Gillot's group demonstrated that the electrochemical behavior of nanostructured nickel nitride against lithium delivers a specific capacity of about 1200 mA h g^{-1}. [21] Despite the aforementioned efforts, there are still no reports on cubic NiN as an anode material in LIBs. Specifically, the studies of the mechanism of lithium-ion intercalation and the dynamics of lithium-ion migration in cubic NiN have not been reported to date.

Commonly, the conversion reaction could occur upon Li-ion intercalation for such a metal nitride anode material. Two step reactions occur during Li-ion intercalation within nickel nitrides (the charge process and ion conversion process):

$$NiN + xLi \rightarrow Li_xNiN \qquad\qquad (1),$$
$$Li_xNiN + (3-x)Li \rightarrow Ni + Li_3N \qquad\qquad (2),$$

Where Li_xNiN is the intermediate phase of conversion reaction. Usually, an insertion process (step 1) occurs prior to the conversion reaction (step 2) in the common electrode reaction process. The step (1) and (2) reactions make use of all valences of metal cations, thus produce high energy density. To understand the reaction mechanism of lithium ions in cubic NiN, it is necessary to study the Li_xNiN as an intermediate phase of the conversion reaction during lithium-ion intercalation. In this paper, the studies of the electronic structures and lithium-ion migration properties of Li_xNiN were carried out from the first principles calculations. The aim of this work is to obtain fundamental information regarding Li_xNiN to understand the fundamental physics and reveal the possible lithium intercalation mechanism from the atomic level.

2. COMPUTATIONAL DETAILS

All calculations are performed using the Vienna *ab initio* simulation program (VASP) [22-23]. It is depicted as the exchange-correlation part with the generalized gradient approximation (GGA) by

Perdew–Burke–Ernzerhof (PBE) [24]. A 6×6×6 Monkhorst-Pack grid is used for the integration of the Brillouin zone [25]. The choice of the cutoff energy for the expansion of the plane-wave basis set is tested. In the present calculations, a cutoff energy of 550 eV is employed with the total energy converging within 0.01 eV/atom. The $1s^12s^12p^1$, $2s^22p^3$, and $3d^84s^2$ valence electrons are employed for Li, N and Ni, respectively. The atomic positions are fully relaxed and the forces on each atom are less than 0.01 eV/Å. To address the strong electron–electron correlation effects, GGA+U schemes are used with the effective U value of 4.0 eV for the Ni atom. This value has been successfully applied in other systems [26-27]. Typically, in Ref. [26], the value of U is 5 eV, and J is 1 eV; thus, the effective Hubbard parameter $U_{eff} = U - J$ equals 4 eV for Ni. For all the calculations, spin-polarization has been taken into account. The lithium-ion migration pathway and the corresponding energy barriers are calculated with the nudged elastic band (NEB) method. [28]

The structure of the supercell Ni_4N_4 is first constructed and optimized, and then the intermediate phase of the conversion reaction $Li_xNi_4N_4$ (x=1-8) is studied. To study the thermodynamic stability of $Li_xNi_4N_4$ (x=1-8), Li intercalation energies are calculated by

$$E = \frac{1}{X}\left(E_{Li_xNi_4N_4} - E_{Ni_4N_4} - xE_{Li}\right) \qquad (1),$$

where $E_{Li_xNi_4N_4}$ and $E_{Ni_4N_4}$ are the total energy of $Li_xNi_4N_4$ and Ni_4N_4, respectively, E_{Li} is the total energy of the body centered cubic (bcc) Li metal structure (-1.903 eV based on our calculations), and x is the amount of intercalated Li.

3. RESULTS AND DISCUSSION

3.1 Structures and stabilities of $Li_xNi_4N_4$

Figure 1. The optimized structures of (a) Ni_4N_4, (b) $Li_1Ni_4N_4$-Oh (octahedral interstitial site occupation), and (c) $Li_1Ni_4N_4$-Th (tetrahedral interstitial site occupation).

Fig. 1 shows the optimized geometric structure of cubic Ni_4N_4, where the Ni atoms form a closed tetrahedron, and the N atoms occupy the vertex of the tetrahedron and are shared by the vertices of four tetrahedrons. Our optimized equilibrium lattice constant is 4.260 Å. As an anode material of lithium-ion batteries, Ni_4N_4 is accompanied by the insertion and removal of lithium ions during the

charge and discharge process. Obviously, there are two kinds of lithium-ion interstitial sites in the Ni_4N_4 compound, that is, the octahedral interstitial site (O_h) $Li_1Ni_4N_4$-Oh and the tetrahedral interstitial site (T_h) $Li_1Ni_4N_4$-Th, as shown in Fig. 1. The calculated total energies of the octahedral and tetrahedral interstitial sites when one lithium ion inserts into Ni_4N_4 are -43.836 eV and -43.258 eV, respectively, indicating that the structure of the octahedral interstitial site occupation is more stable thermodynamically than that of the tetrahedral interstitial site occupation. Lithium ions prefer to occupy the octahedral interstitial sites, which are conducive to the formation of more interstitial Li in the octahedral interstitial site.

Fig. 2 depicts the equilibrium structures of the $Li_xNi_4N_4$ (x=1-8) compounds. It is clear that lithium ions first occupy the octahedral interstitial site and then occupy the tetrahedral interstitial site. In addition, the unit cell volumes, theoretical specific capacity, and lithium intercalation energies of $Li_xNi_4N_4$ (x=0-8) are calculated and listed in Table 1.
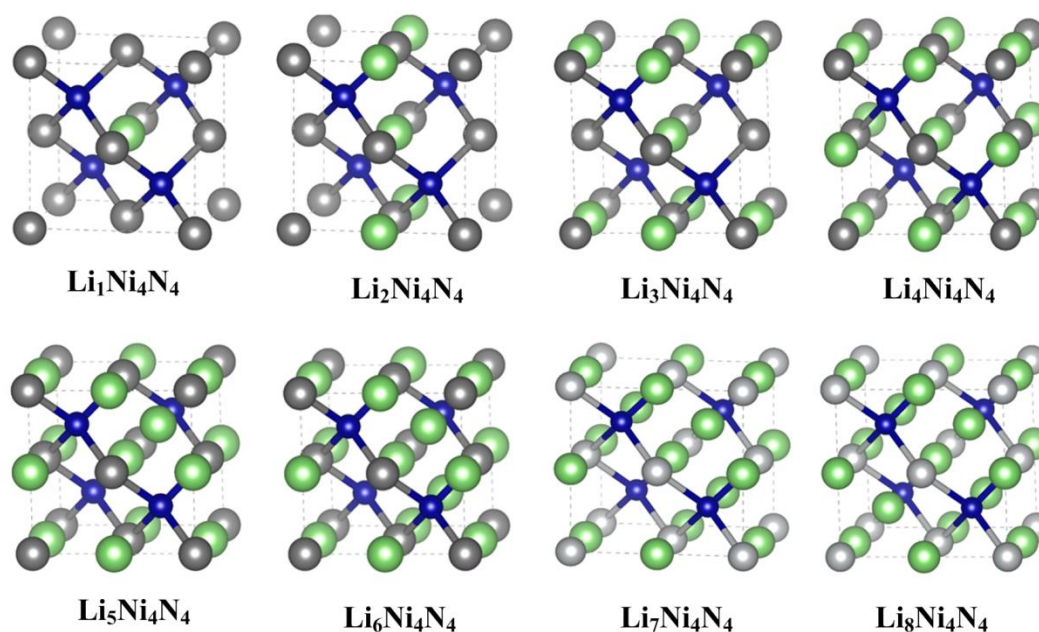
Figure 2. The optimized structures of $Li_xNi_4N_4$ (x=1-8).

Apparently, after full relaxation, there is a serious volume expansion with the insertion of lithium ions. Moreover, it can be found that the lithium intercalation energies decrease first from -0.410 eV for $Li_1Ni_4N_4$ to -1.108 eV for $Li_4Ni_4N_4$ for the octahedral interstitial site occupations. This decrease can be explained by the strengthened interaction between the inserted lithium ions and the lattice.

Then, the repulsive force between the inserted lithium ions becomes dominant, resulting in an increase in the lithium intercalation energies as x increases from 5 to 8. Notably, the intercalation energy of $Li_8Ni_4N_4$ is only -0.065 eV, indicating that the ternary $Li_8Ni_4N_4$ phase is less stable. That is, it is very difficult to insert the eighth lithium ion into Ni_4N_4. Thus, we conclude that the maximum amount of lithium intercalation in cubic Ni_4N_4 is seven lithium ions. The corresponding theoretical

specific capacity is 644.8 mAh/g. This capacity is much higher than that of commercial graphite (theoretical value: 372 mAh/g) [29–33].

Table 1. Volume ($Å^3$), theoretical specific capacity (mAh/g), and intercalation energies (eV) of $Li_xNi_4N_4$ (*x*=1-8) compounds.

Molecular formula	Volume	Theoretical specific capacity	Intercalation energy
Ni_4N_4	77.31	—	—
$Li_1Ni_4N_4$	84.05	92.1	-0.410
$Li_2Ni_4N_4$	95.17	184.2	-0.730
$Li_3Ni_4N_4$	102.69	276.4	-0.952
$Li_4Ni_4N_4$	106.49	368.5	-1.108
$Li_5Ni_4N_4$	116.55	460.6	-0.869
$Li_6Ni_4N_4$	124.87	552.7	-0.546
$Li_7Ni_4N_4$	129.60	644.8	-0.532
$Li_8Ni_4N_4$	133.60	737.0	-0.065

Table 2. The intercalation energies (eV) of $Li_xNi_{16}N_{16}$ (*x*=28-32) compounds.

$Li_{28}Ni_{16}N_{16}$	$Li_{29}Ni_{16}N_{16}$	$Li_{30}Ni_{16}N_{16}$	$Li_{31}Ni_{16}N_{16}$	$Li_{32}Ni_{16}N_{16}$
-0.523	-0.480	-0.340	-0.243	-0.038

In addition, to probe the converged value of Li intercalation in the NiN system, the supercell of 2×2×1 ($Ni_{16}N_{16}$) is formed to test the actual percentage of Li intercalation in the NiN system. The test calculations from $Li_{28}Ni_{16}N_{16}$ are conducted and correspond to only the $Li_7Ni_4N_4$ system. The intercalation energies of $Li_xNi_{16}N_{16}$ (*x*=28-32) are listed in Table 2, and the corresponding structures of $Li_xNi_{16}N_{16}$ (*x*=28-32) are shown in Fig. 3.
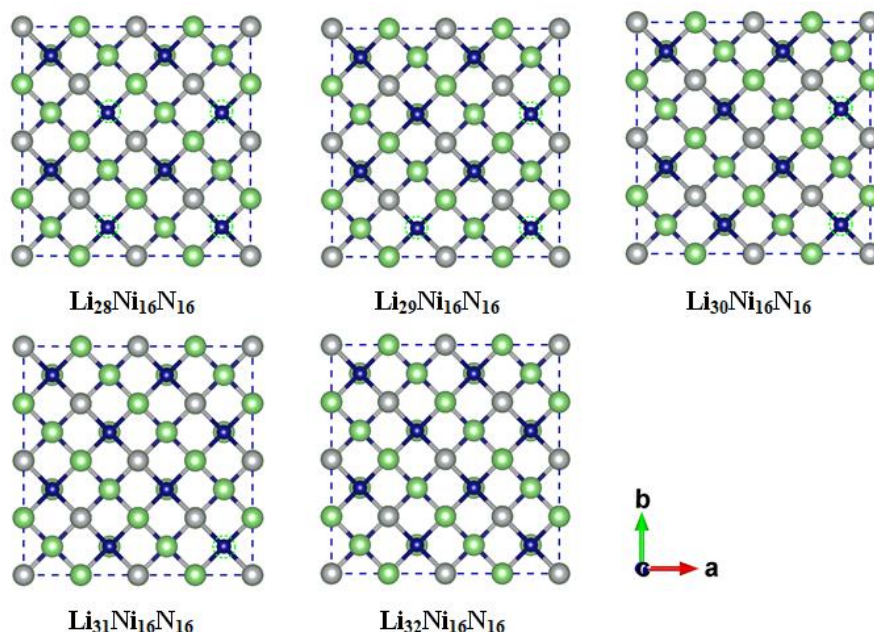
Figure 3. The optimized structures of $Li_xNi_{16}N_{16}$ (x=28-32). The dotted green circle denotes the Li vacancy.

From the intercalation energies, we also believe that it is very difficult for the 32nd Li to be inserted in $Ni_{16}N_{16}$. Thus, the maximum amount of lithium intercalation in cubic $Ni_{16}N_{16}$ is 31 lithium ions. The corresponding theoretical specific capacity is 713.9 mAh/g. This capacity is higher than the first-cycle capacity of CrN nanoparticles (635 mAhg^{-1}), [34] TiN nanowires (567 mAhg^{-1}), [35] and stoichiometric germanium nitride (500 mAhg^{-1}), [36] however it is lower than the specific capacity of nanostructured NiN (1200 mAhg^{-1}), [21] CoN (1100 mAhg^{-1}), [37] and CoN nanoparticles (1290 mAhg^{-1}). [38]

3.2 Electronic structures of $Li_xNi_4N_4$

To understand the effects of Li intercalation on the electronic structure and bonding nature of cubic Ni_4N_4, the energy bands and densities of states (DOS) of $Li_xNi_4N_4$ (x=0-8) are calculated. Typically, the selected electronic structures of Ni_4N_4, $Li_1Ni_4N_4$, and $Li_4Ni_4N_4$ are drawn in Fig. 4 (a)-(f). Fig. 4 (a) and (d) show the energy band, total and projected densities of states of the pristine Ni_4N_4 anode material. From the band structure, it is clear that Ni_4N_4 has a typical metallic conductivity and the conducting electrons are completely spin nonpolarized in this material. The analysis of PDOS exhibits that the electronic states at the Fermi level are mainly contributed by the 3d orbitals of the Ni atoms and the 2p orbitals of the N atoms. Upon insertion of one lithium ion, Fig. 4 (b) and (e) indicate that there is a small spin polarization in $Li_1Ni_4N_4$ with the magnetic moment of 1.1 μ_B. For the intercalation of four lithium ions, Fig. 4 (c) and (f) show the calculated electronic band structures and DOS of $Li_4Ni_4N_4$. Clearly, there are spin nonpolarized electrons in $Li_4Ni_4N_4$ with a 0.0 μ_B magnetic moment; thus, the conducting electrons are also spin nonpolarized electrons. This effect may be due to the high symmetry of the $Li_4Ni_4N_4$ system.

Importantly, from Fig. 4 (e) and (f), the DOS at the Fermi level of $Li_1Ni_4N_4$ and $Li_4Ni_4N_4$ are dominated by the 2p orbitals of the N atoms and the 3d orbitals of the Ni atoms, and the electronic states of Li are almost negligible.
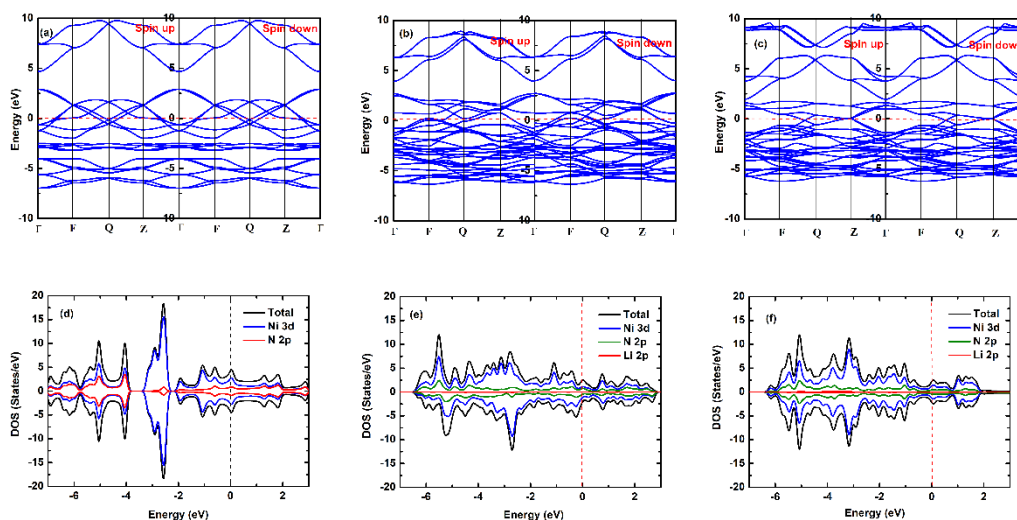
Figure 4. Calculated bands and density of states of Ni_4N_4 (a) and (d), $Li_1Ni_4N_4$ (b) and (e), and $Li_4Ni_4N_4$ (c) and (f), dash lines denote the Fermi level.
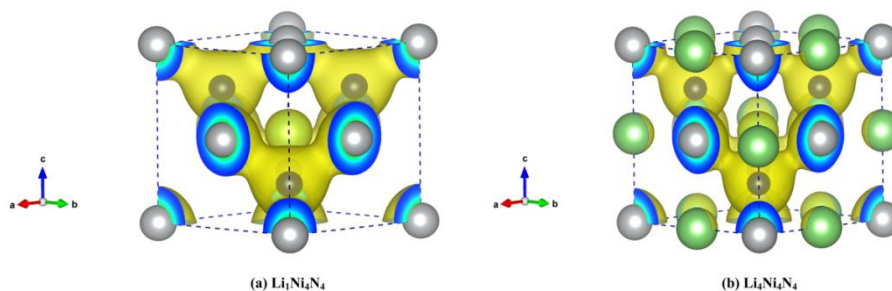
Figure 5. Calculated total charge density distribution of $Li_1Ni_4N_4$ (a) and $Li_4Ni_4N_4$ (b).
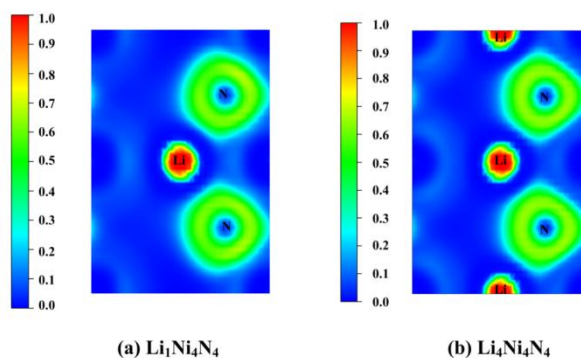
Figure 6. Calculated electron localization function maps for $Li_1Ni_4N_4$ (a) and $Li_4Ni_4N_4$ (b). The illustrations refer to the (110) plane.

This behavior suggests that the bonding states are formed by the strong hybridization of Ni 3d and N 2p orbitals, and the intercalated lithium ions have almost no interactions with N 2p and Ni 3d orbitals, which can facilitate the migration of lithium ions in bulk NiN.

For further insight into the bonding nature, the charge density population and electron localization function (ELF) are investigated. Herein, two kinds of lithium intercalation concentrations, namely, $Li_1Ni_4N_4$ and $Li_4Ni_4N_4$ are selected to show the bonding characteristics. Fig. 5 shows the charge density population of $Li_1Ni_4N_4$ and $Li_4Ni_4N_4$. It can be clearly seen that lithium is not involved in the bonding, further showing that the bonding is caused by the hybridization of the Ni 3d and N 2p orbitals. Furthermore, Fig. 6 shows the calculated ELF maps of the (110) plane for $Li_1Ni_4N_4$ and $Li_4Ni_4N_4$. The ELF map is an effective tool to classify the nature of the interactions between atoms and molecules. Obviously, a distinct charge density at the Li site is observed, indicating that Li has a strong localized electronic charge. This behavior again suggests that lithium ions do not participate in bonding with other atoms. Therefore, the lithium ions are expected to move readily during the charging and discharging processes.

3.3 Migration of Li ions in $Li_xNi_4N_4$

Lithium-ion migration dynamics is an important physics problem, which is associated with the speed of the structural phase transition and the rate performance of the anode material. [39] Therefore, it is very important to study lithium-ion diffusion behavior in electrode materials.
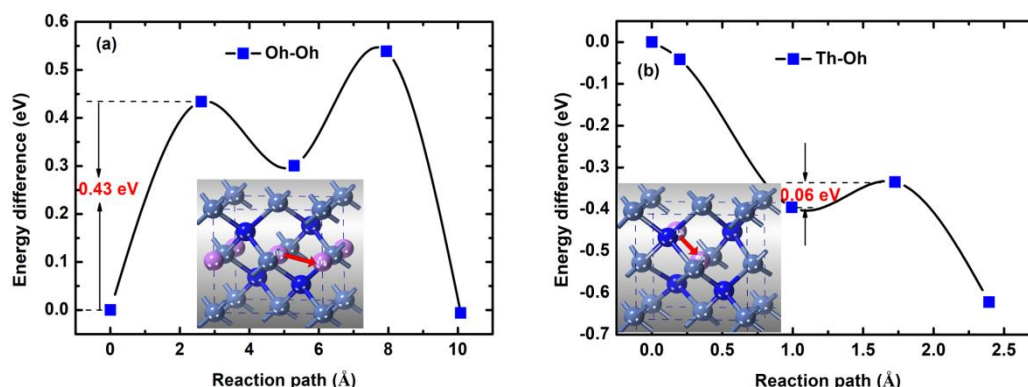
Figure 7. Energy profiles along with the migration pathway of interstitial Li migration from octahedral site to octahedral site (a) and from tetrahedral site to octahedral site (b); O_h and T_h denote the octahedral and tetrahedral sites, respectively.

It is generally known that there are two possible lithium migration mechanisms in the electrode material of a lithium-ion battery, that is, interstitial Li migration and Li vacancy migration. In this work, we only consider interstitial Li migration since Ni_4N_4 is a promising anode material. For interstitial Li in bulk Ni_4N_4, as described above (see 3.1 section), we found that there are two types of stable interstitial sites described as the octahedral interstitial and tetrahedral interstitial sites, and the favorable interstitial site is the octahedral interstitial site. Fig. 7 (a) shows a migration pathway for

single interstitial Li migration from an O_h site to its adjacent O_h site along with the energy barriers. It is shown that the energy barrier of interstitial Li migration in bulk NiN is approximately 0.43 eV, suggesting that interstitial Li migration from an O_h site to an O_h site is allowed for a low Li concentration phase. This is similar to the case of CoN [19], where the Li-ion migrates from the O_h site to the nearest one accompanied the energy barrier of 0.44 eV. Fig. 7 (b) shows single interstitial Li migration pathway from a T_h site to its adjacent O_h site and its energy profile. Obviously, the migration of interstitial Li from a tetrahedral position to an adjacent octahedral site only needs to overcome 0.06 eV. This finding again shows that the tetrahedral interstitial site is thermodynamically less stable than the octahedral interstitial site.

4. CONCLUSIONS

The electronic structures and diffusion behaviors of Li intercalation in bulk Ni_4N_4 are studied by using first principles calculations. The results show that intercalated lithium ions more favorably occupy octahedral interstitial sites than tetrahedral interstitial sites in cubic Ni_4N_4. The systems undergo a serious volume expansion with an increasing Li intercalation concentration. According to the Li intercalation energies, it is concluded that the maximum amount of lithium intercalation is $Li_7Ni_4N_4$. The corresponding theoretical specific capacity reaches 644.8 mAh/g, which is far higher than that of commercial graphite. Upon using a larger supercell of $Ni_{16}N_{16}$, the theoretical specific capacity can be accurate to 713.9 mAh/g. Further analysis of the bands and DOS of selected $Li_1Ni_4N_4$ and $Li_4Ni_4N_4$ shows that the electronic states at the Fermi level are mainly contributed by the Ni 3d and N 2p orbitals, and the contribution of Li is almost zero, which indicates that lithium ions are not involved in bonding. This effect can help the migration of lithium ions in bulk NiN. The calculated charge density population and ELF also confirm this conclusion. Finally, interstitial Li migration is investigated. The results show that the interstitial Li migration from an O_h site to an O_h site does need to overcome the energy barrier of 0.43 eV.

References

1. Z. Song and H. Zhou, *Energy Environ. Sci.,* 6 (2013) 2280-2301.
2. Z. Wang and L. Zhou, *Adv. Mater.,* 24 (2012) 1903-1911.
3. G. Cui, L. Gu, A. Thomas, L. Fu, P. A. van Aken, M. Antonietti, and J. Maier, *ChemPhysChem,* 11 (2010) 3219-3223.
4. G. Wang, X. Shen, J. Yao and J. Park, *Carbon,* 47 (2009) 2049-2053.
5. B. Guo, X. Wang, P. F. Fulvio, M. Chi, S. M. Mahurin, X. G. Sun and S. Dai, *Adv. Mater.,* 23 (2011) 4661.
6. J. Chen, L. N. Xu, W. Y. Li and X. L. Gou, *Adv. Mater.,* 17 (2005) 582–586.
7. L. Li, A. R. O. Raji and J. M. Tour, *Adv. Mater.,* 25 (2013) 6298-6302.
8. S. Dong, X. Chen, X. Zhang and G. Cui, *Coord. Chem. Rev.,* 257 (2013) 1946–1956.
9. D. Tang, R. Yi, M. L. Gordin, M. Melnyk, F. Dai, S. Chen, J. Song and D. Wang, *J. Mater. Chem. A.,* 2 (2014) 10375.
10. S. Dong, X. Chen, L. Gu, X. Zhou, H. Wang, Z. Liu, P. Han, J. Yao, L. Wang, G. Cui and L. Chen, *Mater. Res. Bull.,* 46 (2011) 835–839.
11. Q. Sun and Z. W. Fu, *Electrochim. Act.,* 54 (2008) 403–409.
12. D. K. Nandi, U. K. Sen, D. Choudhury, S. Mitra and S. K. Sarkar, *ACS Appl. Mater. Interfaces,* 6

(2014) 6606–6615.

13. Q. Sun and Z. W. Fu, *Electrochem. Solid-State Lett.*, 11 (2008) A233–A237.
14. D. Choi and P. N. Kumta, *J. Am. Ceram. Soc.* 94 (2011) 2371–2378.
15. D. Choi and P. N. Kumta, *J. Am. Ceram. Soc.* 90 (2007) 3113–3120.
16. M. V. Reddy, G. Prithvi, K. P. Loh and B. V. R. Chowdari, *ACS Appl. Mater. Interfaces,* 6 (2014) 680–690.
17. D. D. Kun, F. Krumeich, R. Fotedar and R. Nesper, *J. Power Sources,* 278 (2015) 608-613.
18. K. J. Zhang, H. B. Wang, X. Q. He, Z. Liu, L. Wang, L. Gu, H. X. Xu, P. X. Han, S. M. Dong, C. J. Zhang, J. H. Yao, G. L. Cui and L. Q. Chen, *J. Mater. Chem.,* 21 (2011) 11916-11922.
19. H. B. Wang, X. L. Song, Y. Xu and Z. H. Yang, *Mod. Phys. Lett. B.,* 32 (2018) 1850184.
20. Z. Stoeva, R. Gomez, A. G. Gordon, M. Allan, D. H. Gregory, G. B. Hix and J. J. Titman, *J. Am. Chem. Soc.,* 126 (2004) 4066–4067.
21. F. Gillot, J. Oró-Solé and M. R. Palacín, *J. Mater. Chem.,* 21 (2011) 9997–10002.
22. G. Kresse and J. Hafner, *Phys. Rev. B.,* 47 (1993) 558.
23. G. Kresse and J. Furthmüller, *Phys. Rev. B.,* 54 (1996) 11169.
24. J. P. Perdew, K. Burke and M. Ernzerhof, *Phys. Rev. Lett.,* 77 (1996) 3865−3868.
25. H. J. Monkhorst and J. D. Pack, *Phys. Rev. B.,* 13 (1976) 5188−5192.
26. D. Das and S. Ghosh, *J. Phys. D: Appl. Phys.,* 48 (2015) 425001.
27. I. M. Ndassa, M. Gilleßen, B. P. T. Fokwa, *Solid State Sci.,* 17 (2013) 14.
28. G. Enkelman, B. P. Uberuaga and H. Jónsson, *J. Chem. Phys.*, 113 (2000) 9901.
29. G. A. Nazri and G. Pistoia, ed. Kluwer Academic Publ. New York. 2003.
30. P. G. Bruce, B. Scrosati and J. M. Tarascon, *Angew. Chem. Int. Ed.,* 47 (2008) 2930-2946.
31. Y. Q. Sun, Q. O. Wu and G. Q. Shi, *Energy Environ. Sci.,* 4 (2011) 1113-1132.
32. J. Cabana, L. Monconduit, D. Larcher and M. R. Palacin, *Adv. Mater.,* 22 (2010) E170-E192.
33. J. Hassoun, K. S. Lee, Y. K. Sun and B. Scrosati, *J. Am. Chem. Soc.,* 133 (2011) 3139-3143.
34. B. Das, M. V. Reddy, G. V. Subba Rao and B. V. R. Chowdari, *RSC Adv.*, 2 (2012) 9022–9028.
35. M.-S. Balogun, M. Yu, C. Li, T. Zhai, Y. Liu, X. Lu and Y. Tong, *J. Mater. Chem. A*, 2 (2014) 10825–10829.
36. N. Pereira, M. Balasubramanian, L. Dupont, J. McBreen, L. Klein and G. Amatucci, *J. Electrochem. Soc.*, 150 (2003) A1118–A1128.
37. M. V. Reddy, G. Prithvi, K. P. Loh and B. V. R. Chowdari, *ACS Appl. Mater. Interfaces*, 6 (2014) 680–690.
38. B. Das, M. V. Reddy, G. V. Subba Rao and B. V. R. Chowdari, *J. Mater. Chem.*, 22 (2012) 17505–17510.
39. J. Cabana, Z. Stoeva, J. J. Titman, D. H. Gregory and M. R. Palacin, *Chem. Mater.,* 20 (2008) 1676-1678.